Magnetic, transport, and thermal properties of $Yb_2T_3X_9$ compounds (T=Rh, Ir; X=Al, Ga)

O. Trovarelli, C. Geibel, B. Buschinger, R. Borth, S. Mederle, M. Grosche, G. Sparn, and F. Steglich
Max-Planck-Institut of Chemical Physics of Solids, D-01187 Dresden, Germany

O. Brosch and L. Donnevert
Institute of Solid State Physics, Technical University of Darmstadt, D-64289 Darmstadt, Germany
(Received 30 October 1998; revised manuscript received 9 February 1999)

The low-temperature properties of a family of ytterbium-based compounds with the composition $Yb_2T_3X_9$ (T=Rh, Ir; X=Al, Ga) are studied by means of magnetic susceptibility, electrical resistivity, thermoelectric power, and specific-heat C_P measurements. $Yb_2Rh_3Al_9$ and $Yb_2Ir_3Al_9$ show the typical properties of heavy-fermion antiferromagnets, namely they order at T_N=3.5 K and T_N=5.5 K, respectively, their C_P/T data extrapolate to γ_o=230 mJ/mol Yb K^2 below 0.5 K, and their entropy gain at T_N reaches $0.6R \ln 2$ only. The transport data show evidence of low-lying crystal-electric-field levels separated by $\Delta_{CEF} \simeq 30$ K from the ground-state doublet. On the contrary, $Yb_2Rh_3Ga_9$ and $Yb_2Ir_3Ga_9$ show mixed-valent behavior, as observed in most Yb-based intermetallics. The effect of the ligands on the ground-state properties is discussed and compared with other lanthanide- and actinide-based isostructural $R_2T_3X_9$ homologues. [S0163-1829(99)12225-2]

I. INTRODUCTION

The observation of the onset of superconductivity and of non-Fermi-liquid effects at the transition between a magnetic ordered (MO) and nonmagnetic ground state (GS) has reattracted considerable interest in the study of Kondo lattices (KL).[1] Whereas a tremendous amount of information is presently available for Ce-based KL, rather little effort has been devoted to investigate KL systems based on Yb, probably because of the difficult task of the sample preparation.[2] Moreover, most of all known Yb-based intermetallics are found in a mixed-valent (MV) regime and, in comparison to Ce systems, there is a relatively few number of Yb-based compounds showing the typical properties of MO-KL or heavy fermions.[2,3] In these three-dimensional array of ($4f$ or $5f$) moments embedded in a metallic environment, the nature of the GS is generally considered to result from a competition between intrasite Kondo effect [with a characteristic energy given by the Kondo temperature $k_BT_K \propto \exp(-1/|\mathcal{J}|)$] and intersite magnetic RKKY-type interactions (described as $k_BT_{RKKY} \propto \mathcal{J}^2$).[4] The final balance between these two mechanisms is driven by the strength $\mathcal{J}$ of the hybridization between the f and conduction electrons. Within this model, magnetic order of eventually reduced moments by the Kondo effect is expected to occur for $T_{RKKY} > T_K$, heavy-fermion behavior for $T_{RKKY} \simeq T_K$, whereas MV behavior for $T_K \gg T_{RKKY}$.

We present here a detailed study of two MO Yb-based KL compounds: $Yb_2T_3Al_9$ (T=Rh, Ir). On the contrary, the Ga-based homologues $Yb_2T_3Ga_9$ behave as ''typical'' MV compounds. Besides being interesting because of their own properties, these compounds present the advantage of allowing a comparison with isostructural Ce- and U-based compounds formed with the same ligands, which show unusual low-temperature properties as well.

The $R_2T_3X_9$ series of compounds (where R=lanthanide or the actinide uranium, T=transition element, and X=p element like Al or Ga) was first observed by Grin *et al.*[5,6] who determined their crystallographic structure ($Y_2Co_3Ga_9$-type). Despite this orthorhombic structure (space group $Cmcm$) has a relatively large number of atoms per unit cell, it is an ordered structure with only one equivalent crystallographic site for the R component. Very recently, Buschinger *et al.*[7–9] investigated the low-temperature properties of a number of $R_2T_3X_9$ compounds formed with R=La, Ce, and U, in combination with T=Rh, Ir and X=Al, Ga. The four studied Ce-based compounds are nonmagnetic and present rather unusual GS properties. Their magnetic response shows the typical behavior of MV compounds like, e.g., $CeSn_3$,[10] but their low-temperature transport and thermal properties resemble the behavior of heavy-fermion systems like, e.g., $CeRu_2Si_2$.[11–13] Very recent neutron diffraction experiments on $Ce_2Rh_3Al_9$ confirm the absence of magnetic reflections down to 1.8 K.[14] Moreover, low-temperature measurements of the magnetization density reveal a complete localization of the magnetic moments at the Ce site, with no residual magnetization on any other site larger than $\sim$3% of the total moment.[14] Although a satisfactory explanation of the behavior of Ce in these compounds is still missing, this unconventional situation might invoke the necessity of a description in terms of two different energy scales for the same $4f$ electrons.[9] On the contrary, the U-based counterparts appear as rather conventional MO systems with ordering temperatures between 8 K and 35 K,[8] despite the fact that an interpretation of their GS properties in terms of an itinerant behavior of the $5f$-U electrons cannot be ruled out.[7]

The interesting properties of the Ce and U compounds deserve to extend the study to other members of the $R_2T_3X_9$ family, in particular to those formed with R=Yb, for Yb^{3+} in its $4f^{13}$ electronic configuration, can be considered as analogous in terms of holes to the $4f^1$ configuration of Ce^{3+} with one $4f$ electron.[15] Since the unique low-temperature behavior of the Ce-based $R_2T_3X_9$ compounds appears to be linked to the presence of a nearby magnetic instability (i.e., a phase transition between nonmagnetic and MO-GS),[9] ac-

TABLE I. Values of the lattice parameters and unit-cell volumes of the $Yb_2R_3X_9$ compounds (orthorhombic $Y_2Co_3Ga_9$-type structure, space group $Cmcm$). The data of Grin *et al.* (Ref. 6) for X = Ga are included in parentheses for comparison.

	$Yb_2Rh_3Al_9$	$Yb_2Ir_3Al_9$	$Yb_2Rh_3Ga_9$	$Yb_2Ir_3Ga_9$
a [Å]	12.906	12.927	13.050 (12.949)	12.968 (12.982)
b [Å]	7.542	7.483	7.487 (7.480)	7.502 (7.596)
c [Å]	9.381	9.367	9.400 (9.453)	9.450 (9.443)
V [Å^3]	913.13	906.13	918.4 (915.6)	919.37 (931.18)

cording to this electron-hole analogy, one can expect the Yb counterparts to present interesting low-temperature properties as well.

After describing the experimental and crystallographic details in Sec. II, the magnetic, transport, and thermal properties of the MO-KL $Yb_2T_3Al_9$ (T=Rh, Ir) are presented in Sec. III. The properties of the Ga-based $Yb_2T_3Ga_9$ (T =Rh, Ir) are described in Sec. IV. The paper is concluded in Sec. V, where we analyze the GS properties of these compounds and compare them with those of other lanthanide- and actinide-based isostructural $R_2T_3X_9$ homologues.

II. EXPERIMENTAL DETAILS

Polycrystalline samples were prepared by melting stoichiometric amounts of R=Yb; T=Rh or Ir; and X=Al or Ga using the closed Ta-crucible technique, as described elsewhere.[16] The purity of the constituents varies from 3N for Rh and Ir, to 7N in the case of Ga. Heating temperatures of the order of 1400 °C during some minutes were enough to obtain homogeneous samples. After the melting procedure the samples were annealed inside the Ta crucible at 800 °C for two weeks in order to assure good homogenization. The crystallographic characterization was performed by means of x-ray powder diffractometry using Si as an internal standard. All of them were confirmed to crystallize in the orthorhombic $Y_2Co_3Ga_9$-type structure.[6,7] We detect the presence of the order of 2% of impurity phases in the worst cases, i.e., for $Yb_2Rh_3Ga_9$. The values of the lattice constants as well as the volumes of the unit cells are displayed in Table I.

In order to characterize the physical properties we used standard experimental techniques. Magnetic susceptibility χ and magnetization M measurements on fine-powder samples were performed in a commercial SQUID magnetometer in the temperature range 2 K$<T<$350 K and in magnetic fields up to B=5.5 T. To this end, ~0.1 g of fine powder were mixed with a small amount of paraffin in closed gelatin capsules. After melting the wax inside the magnetometer (at 330 K) the mixture was cooled down, either in zero-field or in B=5 T to obtain random- or oriented-powder, respectively. The (almost negligible) magnetic contribution of capsule and wax was subtracted afterwards to obtain the final χ or M results. The Seebeck coefficient (or thermoelectric power, TEP) was measured on bars using a steady-state method, as described elsewhere.[9] The dc electrical-resistivity $\rho(T)$ data were taken simultaneously with the TEP in the range 2 K$<T<$300 K. Additional $\rho(T)$ measurements down to 0.5 K were performed in a ^{3}He cryostat using the ac four-probe technique. The specific-heat C_P was measured in a semiadiabatic ^{3}He calorimeter using the heat-pulse method in temperatures 0.5 K$<T<$10 K and in fields up to 4 T.

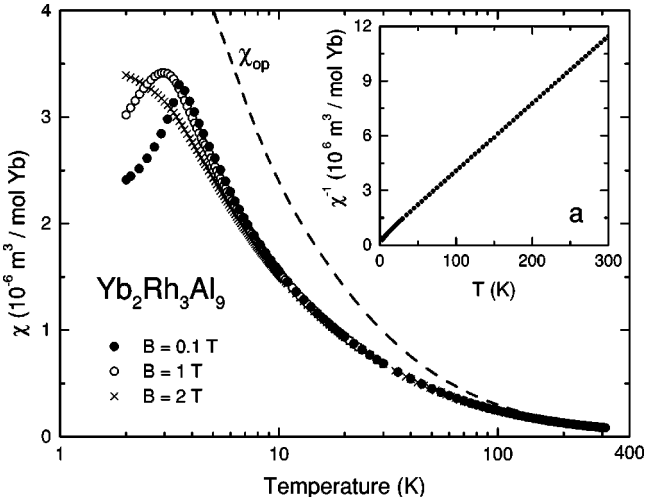

FIG. 1. Magnetic susceptibility χ_{poly} of $Yb_2Rh_3Al_9$ in a log-T scale in different applied magnetic fields. The dotted line represents χ_{op} in B=0.1 T for $T>T_N$, as explained in the text. (a) Inverse susceptibility $\chi^{-1}_{poly}(T)$ in B=0.1 T as a function of temperature.

III. MAGNETIC KONDO-LATTICE BEHAVIOR IN $Yb_2Rh_3Al_9$ AND $Yb_2Ir_3Al_9$

A. Magnetic properties

The mean value of the magnetic susceptibility was measured on random-powder, as described above. This procedure eliminates any preferred orientation of the grains in the bulk and allows to simulate a measurement on an isotropic polycrystalline sample, hereafter χ_{poly}. The results are presented in Fig. 1 and Fig. 2 for $Yb_2Rh_3Al_9$ and $Yb_2Ir_3Al_9$, respectively. At high temperatures $\chi^{-1}_{poly}(T)$ of both compounds reveal a Curie-Weiss (CW) behavior, described by effective magnetic moments $\mu_{eff}=4.2\mu_B$ and $\mu_{eff}=4.3\mu_B$, and extrapolated CW paramagnetic temperatures $\Theta_P=-10$ K and $\Theta_P=-18$ K for $Yb_2Rh_3Al_9$ and $Yb_2Ir_3Al_9$,

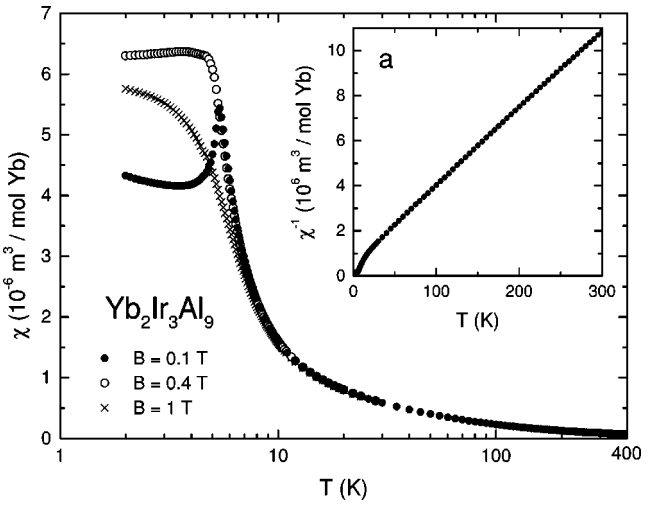

FIG. 2. Magnetic susceptibility χ_{poly} of $Yb_2Ir_3Al_9$ in a log-T scale in different applied magnetic fields. (a) Inverse susceptibility in B=0.1 T as a function of temperature.

TABLE II. Summary of the experimental data of the $Yb_2T_3X_9$ compounds: magnetic ordering temperature T_N, effective magnetic moment $\mu_{\rm eff}$, Curie-Weiss temperature Θ_P, temperature of the maximum in the electrical resistivity $T_{\max,\rho}$, of the minimum $T_{\min,\rm TEP}$ and maximum $T_{\max,\rm TEP}$ of the Seebeck coefficient, maximum in the susceptibility $T_{\max,\chi}$, extrapolated γ_o coefficient, entropy gain ΔS at T_N, and estimated value of the Kondo temperature T_K.

	$Yb_2Rh_3Al_9$	$Yb_2Ir_3Al_9$	$Yb_2Rh_3Ga_9$	$Yb_2Ir_3Ga_9$
T_N [K]	3.5	5.5		
$\mu_{\rm eff}$ [μ_B/Yb]	4.2	4.3		
Θ_P [K]	−10	−18		
$T_{\max,\rho}$ [K]	23	20		
$T_{\min,\rm TEP}$ [K]	30; 2	40		
$T_{\max,\rm TEP}$ [K]	5	4.5		
$T_{\max,\chi}$ [K]			120	250
γ_o [mJ/mol Yb K^2]	230	225		
$\Delta S(T_N)$ [$R\ln 2$]	0.60	0.65		
T_K [K]	2.6	4.1		

respectively. These data are included in a summary of the experimental results in Table II. The $\mu_{\rm eff}$ values are close to that of free-Yb^{3+} ions (i.e., $\mu_{\rm eff}=4.5\mu_B$), indicating that the GS corresponds to the $^2F^{7/2}$ configuration given by Hund's rules. The deviation from linearity observed below ~ 25 K [in particular for $Yb_2Ir_3Al_9$, see Fig. 2(a)] might be related to the influence of crystal-electric-field (CEF) effects, which are expected to split the $J=7/5$ ground spin-orbit multiplet in four Kramer's doublets.

At low temperatures $\chi_{\rm poly}(T)$ of $Yb_2Rh_3Al_9$ measured in $B=0.1$ T shows a typical antiferromagnetic (AF) transition at $T_N=3.5$ K (see Fig. 1), whereas $Yb_2Ir_3Al_9$ presents an unusually peaked AF-type anomaly at $T_N=5.5$ K that flattens off rapidly below T_N (see Fig. 2). At higher fields both curves evolve into a flat, enhanced susceptibility below 3 K.

Before analyzing the characteristics of the ordered phases of $Yb_2Rh_3Al_9$ and $Yb_2Ir_3Al_9$ we investigate the influence of the magnetocrystalline anisotropy on their paramagnetic susceptibility. This can be estimated by comparing $\chi_{\rm poly}(T)$ with susceptibility measurements on oriented-powder samples $\chi_{\rm op}(T)$, which allows to simulate a measurement along the easy-magnetization direction. Such a comparison provides information about the single-ion anisotropy expected to arise from the local CEF interaction at the R site. The oriented-powder $\chi_{\rm op}(T)$ data of $Yb_2Rh_3Al_9$ are included as a dashed line in Fig. 1, where a ratio $\chi_{\rm op}/\chi_{\rm poly}\sim 1.6$ is observed as T approaches T_N. This value can be taken as an indication that the magnetic anisotropy in $Yb_2Rh_3Al_9$ might be of ''easy-axis'' type, since for an ''easy-axis'' paramagnet one expects $1<\chi_{\rm op}/\chi_{\rm poly}<3$, whereas for an ''easy-plane'' picture $1<\chi_{\rm op}/\chi_{\rm poly}<3/2$ is expected. On the contrary, $\chi(T)$ of $Yb_2Ir_3Al_9$ is observed to be almost isotropic, i.e., $\chi_{\rm op}/\chi_{\rm poly}\sim 1$ in the whole temperature range.

In order to investigate the nature of the magnetic response of $Yb_2Rh_3Al_9$ and $Yb_2Ir_3Al_9$ in more detail, isothermal magnetization curves are plotted in Figs. 3 and 4, respectively. Clear metamagnetic behavior without hysteresis effects is present in $Yb_2Rh_3Al_9$ below T_N. The effect of the metamagnetic transition can be better observed after plotting the derivative $\partial M/\partial B)_T$ vs B in Fig. 3(a). The sharp peak at $B^*\simeq 1$ T ($T=2$ K) corresponds to the field-induced change in the magnetization, which disappears as T_N is reached. The metamagnetic response is weaker in the case of $Yb_2Ir_3Al_9$ (see Fig. 4), with a slight S-shape behavior leading to a broad $\partial M/\partial B)_T$ maximum centered at $B^*\simeq 0.4$ T. At the lowest attainable temperature (i.e., $T=2$ K) and fields $B>3$ T the $M(B)$ curves indicate a tendency to a linear field dependence rather than showing saturation. The value of $M_{\rm poly}$ in $B=5.5$ T reaches $(1.5\pm 0.1)\mu_B$/Yb and $(1.4\pm 0.1)\mu_B$/Yb for $Yb_2Rh_3Al_9$ and $Yb_2Ir_3Al_9$, respectively. These values are lower than the free-ion value $4.5\mu_B$/Yb, and can be taken as an indication of a similar magnitude of the magnetic moment of the GS doublet given by the CEF.

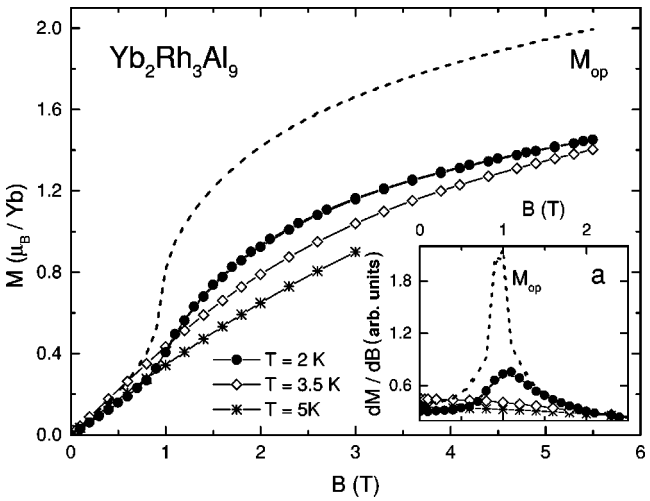

FIG. 3. Isothermal magnetization $M_{\rm poly}$ of $Yb_2Rh_3Al_9$ as a function of field B at $T<T_N$, $T=T_N$, and $T>T_N$, respectively. The isotherm at $T=2$ K of an oriented-powder sample $M_{\rm op}$ (dashed line) is included for comparison. (a) Derivative $\partial M/\partial B)_T$ as a function of field for different temperatures.

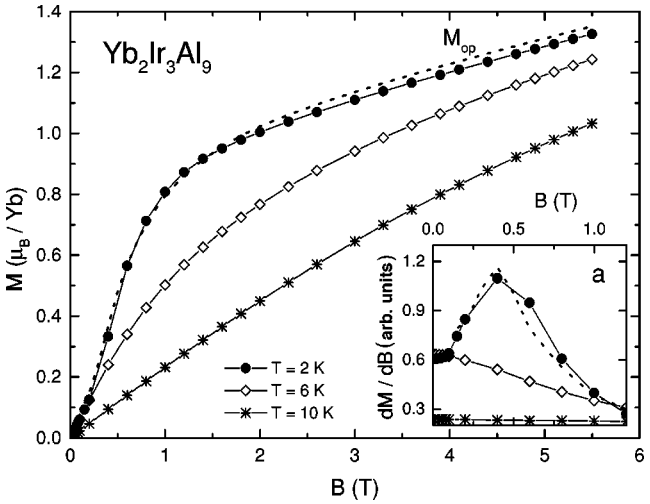

FIG. 4. Isothermal magnetization $M_{\rm poly}$ of $Yb_2Ir_3Al_9$ as a function of field B at $T<T_N$, $T=T_N$, and $T>T_N$, respectively. The $T=2$ K isotherm of an oriented-powder sample $M_{\rm op}$ (dashed line) is included for comparison. (a) Derivative $\partial M/\partial B)_T$ as a function of field for different temperatures.

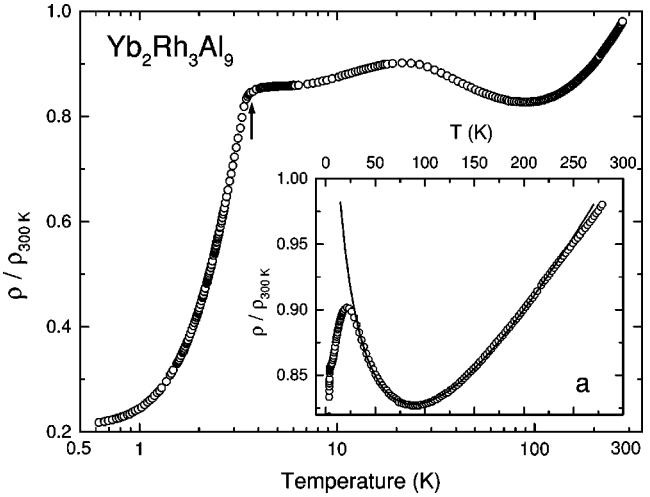

FIG. 5. Electrical resistivity $\rho(T)$ in a log-T scale for $Yb_2Rh_3Al_9$. The arrow indicates the magnetic transition. (a) $\rho(T)$ data in a linear-T scale. The solid line is a fit to the high-temperature data as explained in the text.

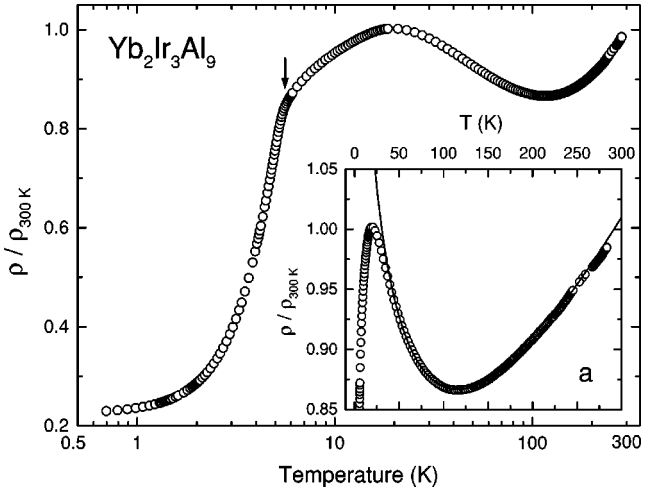

FIG. 6. Electrical resistivity $\rho(T)$ in a log-T scale for $Yb_2Ir_3Al_9$. The arrow indicates the magnetic transition. (a) $\rho(T)$ data in a linear-T scale. The solid line is a fit to the high-temperature data as explained in the text.

A comparison of the $M_{\rm poly}(B)$ isotherm at $T=2$ K with data measured on oriented-powder $M_{\rm op}$ shows that the ratio $M_{\rm op}/M_{\rm poly}$ in $B=5.5$ T reaches ~ 1.5 for $Yb_2Rh_3Al_9$ and $M_{\rm op}/M_{\rm poly}\sim 1$ for $Yb_2Ir_3Al_9$ (cf. Fig. 3 and Fig. 4), being these ratios similar as those observed for the magnetic susceptibility (i.e., $\chi_{\rm op}/\chi_{\rm poly}$) in the paramagnetic state. This observation indicates that the magnetocrystalline anisotropy is also present below T_N and survives up to large fields. Thus, the weak metamagnetic response of $Yb_2Ir_3Al_9$ seems to be connected with its almost isotropic magnetic properties.

The present results regarding the macroscopic magnetic properties of $Yb_2Rh_3Al_9$ and $Yb_2Ir_3Al_9$ are in agreement with preliminary results obtained from very recent neutron-diffraction measurements performed on powder down to 1.5 K.[14,17,18] In the paramagnetic regime, data taken down to $T>T_N$ confirm that the nuclear structure corresponds to the $Cmcm$ space group. At lower temperatures additional intensities due to the onset of magnetic ordering allows to obtain information about the magnetic structure of these compounds. In both cases the magnetic unit cell coincides with the nuclear one and this fact is described by a propagation vector $\vec{k}=(000)$. A quantitative refinement of the intensities indicates that the magnetic structure consists of ferromagnetic $(00l)$ layers at $z=1/4$ and $z=3/4$ which are AF stacked $+-+-$ along the c axis. In the case of $Yb_2Rh_3Al_9$ the magnetic moments are aligned parallel or antiparallel to the c-axis direction, i.e., $+$ for $z=1/4$ and $-$ for $z=3/4$,[17] whereas for $Yb_2Ir_3Al_9$ they are oriented within the a-b plane.[14,18] These results allow to confirm the ''easy-axis'' and the ''easy-plane'' picture deduced from the magnetic measurements for $Yb_2Rh_3Al_9$ and $Yb_2Ir_3Al_9$, respectively

B. Transport properties

The high-temperature dependence of the electrical resistivity of $Yb_2Rh_3Al_9$ and $Yb_2Ir_3Al_9$ are rather similar in many aspects: Starting from room temperature values of the order of 500 $\mu\Omega$ cm, $\rho(T)$ decreases almost linearly with decreasing temperature, as shown in Fig. 5(a) and Fig. 6(a). After showing a minimum at $T\simeq 100$ K, $\rho(T)$ increases as $\rho\propto -\ln T$, down to ~ 25 K, accounting for a large relative ρ increase of $\sim 15\%$ for $Yb_2Ir_3Al_9$. Thus, at high temperatures the total resistivity can be described as $\rho(T)=\rho_o+\rho_{\rm ph}(T)+\rho_{\rm mag}(T)\equiv\rho'+aT-c\ln T$, where ρ_o, $\rho_{\rm ph}$, and $\rho_{\rm mag}$ account for the scattering due to lattice imperfections, phononic and magnetic contributions, respectively.[19] In this equation, $\rho_{\rm mag}$ is the sum of the spin-disorder resistivity and the $(-\ln T)$ Kondo term,[19] whereas a and c are constants. A fit according to this expression reveals satisfactory agreement with the $\rho(T)$ data above ~ 40 K, as shown in Figs. 5(a) and 6(a). Below this temperature maxima are present at $T_{{\rm max},\rho}\simeq 23$ K for $Yb_2Rh_3Al_9$ (Fig. 5) and at $T_{{\rm max},\rho}\simeq 20$ K for $Yb_2Ir_3Al_9$ (Fig. 6), below which $\rho(T)$ decreases rapidly in both compounds.

As the temperature is further decreased and approaches the onset of magnetic ordering a difference is observed between both $\rho(T)$ curves. In the case of $Yb_2Rh_3Al_9$, it tends to flatten off below $T_{{\rm max},\rho}$ and shows an abrupt drop at 3.5 K that develops from almost constant $\rho(T)$ values (Fig. 5). This behavior resembles that of $YbCu_4Au$, in which a sharp and symmetric maximum in $\rho(T)$ at $T_{{\rm max},\rho}\simeq 20$ K is attributed to a competition between incoherent Kondo scattering and low-lying CEF levels.[20] In the case of $Yb_2Ir_3Al_9$, $\rho(T)$ decreases monotonically below $T_{{\rm max},\rho}$ and a kink is present at 5.5 K, below which $\rho(T)$ decreases more rapidly with decreasing temperature (see Fig. 6). The strong reduction of the scattering rate at $T\simeq T_N$ in both compounds is clearly due to the onset of magnetic ordering, corresponding to a relative decrease of $\rho(T)$ below T_N of more than a factor of four, compared to the value of the overall resistance ratio $\rho(300\ {\rm K})/\rho(0.5\ {\rm K})\simeq 5$. Concerning the $\rho(T)$ dependence at low temperatures, it can be described as $\rho\propto T^n$, with $n=2.8$ and $n=2.5$ for $Yb_2Rh_3Al_9$ and $Yb_2Ir_3Al_9$, respectively, suggesting that electron-magnon scattering is the dominant scattering mechanism well below T_N.

The temperature dependence of the TEP of $Yb_2Rh_3Al_9$ and $Yb_2Ir_3Al_9$ also shows comparable trends, as shown in Fig. 7. Starting from small positive values at room tempera-

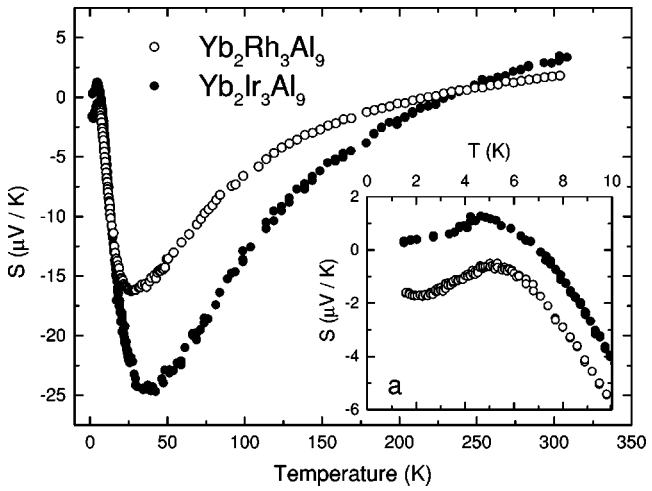

FIG. 7. Thermoelectric power of $Yb_2Rh_3Al_9$ and $Yb_2Ir_3Al_9$ in the temperature range 1.5 K$<T<$300 K. (a) Low-temperature data near T_N.

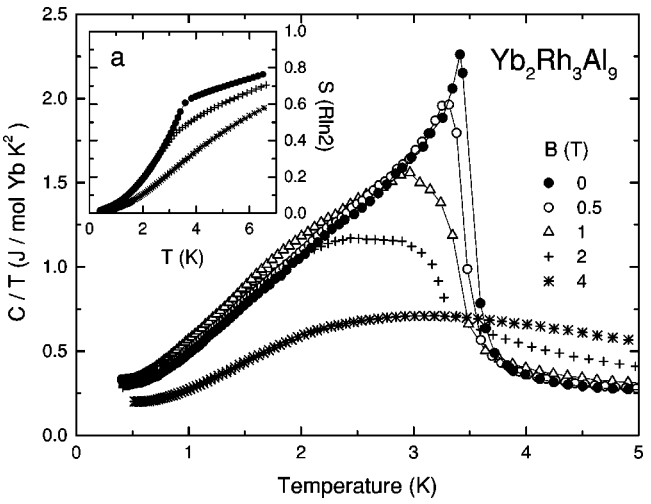

FIG. 8. Low-temperature specific heat divided by temperature of $Yb_2Rh_3Al_9$ measured in $B=0$, 0.5, 1, 2, and 4 T. (a) Entropy gain as a function of temperature for $B=0$, 2, and 4 T.

ture, the sign of the TEP changes at ~ 250 K. For both compounds, TEP decreases with decreasing temperature reaching pronounced minima at $T_{\min,\mathrm{TEP}}=30$ K and 40 K, with rather large negative values of the order of -15 μV/K for $Yb_2Rh_3Al_9$ and -25 μV/K for $Yb_2Ir_3Al_9$, respectively. A shallow maximum is formed for both compounds at $T_{\max,\mathrm{TEP}}\simeq 5$ K. For $Yb_2Rh_3Al_9$, the TEP passes through a clear minimum again at $T_{\min,\mathrm{TEP}}=2$ K [see Fig. 7(a)]. Thus, weak anomalies in the TEP at temperatures close to the respective T_N values might be caused by the onset of magnetic correlations, as predicted in the phenomenological model by Fischer.[21] Both TEP curves are symmetrically similar (with inverted signs) to those of archetypal Ce-based KL-systems.[22] The opposite TEP signs of Yb- and Ce-based systems reflect the hole-electron symmetry of the Yb-4f^{13} and Ce-4f^1 configurations.[15,22]

C. Specific heat

The low-temperature specific-heat data and the entropy gain $\Delta S(T)$ of $Yb_2Rh_3Al_9$ and $Yb_2Ir_3Al_9$ are plotted as C_P/T vs T in Fig. 8 and Fig. 9, respectively. Sharp anomalies at $T_N=3.5$ K (for $Yb_2Rh_3Al_9$) and at $T_N=5.5$ K (for $Yb_2Ir_3Al_9$) correspond to the AF transitions observed in the magnetic and transport properties. Both C_P/T curves at $B=0$ T are quite similar in shape. The only qualitative difference is a broad shoulder at around 2 K for $Yb_2Rh_3Al_9$, despite the marked differences regarding the magnetic anisotropy of both compounds (cf. Sec. III A). In applied magnetic field the transitions at T_N remain sharp up to $B\simeq 0.5$ T, showing slight shifts to lower temperatures as expected for AF transitions. At higher fields the peak at T_N gradually diminishes. An almost ''squared'' shape in C_P/T develops in $B=2$ T for both compounds, and in $B=4$ T only a broad maximum remains.

The C_P temperature dependence for $T<1.5$ K can be described as $C_P/T=\gamma_o+BT^2$, corresponding to the expected dispersion relation of AF magnons. No clear indication of the opening of a gap in the magnon spectrum can be observed down to 0.5 K. The values of γ_o are 230 mJ/mol Yb K^2 for $Yb_2Rh_3Al_9$ and 225 mJ/mol Yb K^2 for $Yb_2Ir_3Al_9$, respectively (see Table II).

IV. MIXED-VALENT BEHAVIOR OF $Yb_2Rh_3Ga_9$ AND $Yb_2Ir_3Ga_9$

The magnetic susceptibility of $Yb_2Rh_3Ga_9$ and $Yb_2Ir_3Ga_9$ are plotted in Fig. 10 as a function of temperature. The $\chi(T)$ curves show rather small absolute values at room temperature in comparison to the $Yb_2R_3Al_9$ compounds, but similar in magnitude as those of prototypical MV systems, like $YbAl_2$ or $YbAl_3$.[23] Their distinctive feature is a broad maximum at temperatures $T_{\max,\chi}\simeq 120$ K for $Yb_2Rh_3Ga_9$ and $T_{\max,\chi}\simeq 250$ K for $Yb_2Ir_3Ga_9$, respectively, characteristic of MV compounds.[16,23,24] Applying the empirical formula $T_{\max,\chi}=2500(3-\nu)$ as proposed by Klaasse *et al.*,[23] which relates the temperature of the maximum of $\chi(T)$ to the Yb valence ν, one obtains $\nu\simeq 2.9+$ for the Ga-based compounds. This situation was already anticipated in Ref. 6,

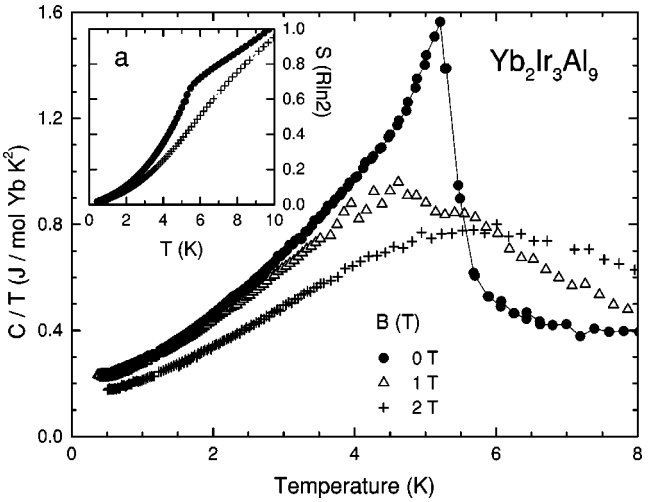

FIG. 9. Low-temperature specific heat divided by temperature of $Yb_2Ir_3Al_9$ measured in $B=0$, 1, and 2 T. (a) Entropy gain as a function of temperature.

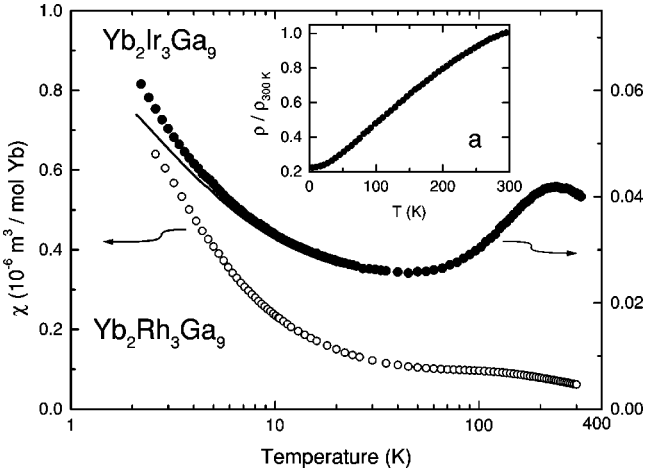

FIG. 10. Magnetic susceptibility in a log-T scale for $Yb_2Rh_3Ga_9$ ($B=0.1$ T) and for $Yb_2Ir_3Ga_9$ in $B=0.1$ T and $B=1$ T (full line). (a) Electrical resistivity $\rho(T)$ of $Yb_2Ir_3Ga_9$ in the temperature range 4 K$<T<$300 K.

where an analysis in terms of the evolution of the unit-cell volume as a function of the R^{3+} ionic radius along the lanthanide series shows a deviation from the general monotonic dependence for $R=$Yb, which hints to a valence state different from $3+$.

At lower temperatures $\chi(T)$ has a minimum at $\sim$50 K, below which $\chi(T)$ increases again leading to a pronounced tail in both compounds. In order to check for the magnetic response of this contribution at low temperatures, the $\chi(T)$ data are compared in Fig. 10 for different applied magnetic fields. A very weak suppression of the low-T tail in higher fields is observed. These tails correspond to a Curie-like temperature dependence for $T<15$ K with an effective moment of 0.27 μ_B/Yb for $B=0.1$ T and 0.29 μ_B/Yb for $B=1$ T, which cannot only be explained by the presence of Yb impurities (mainly Yb_2O_3, Ref. 23). Magnetization curves as a function of field for $Yb_2Ir_3Ga_9$ (not presented here) show that at $T=10$ K, M is linear in B up to 5.5 T, with a slope corresponding to the value of $\chi(T=10\ \text{K})$ of Fig. 10. At $T=2$ K, M shows a slight curvature which can be accounted for the saturation of only a tiny fraction of the order of 0.4% of Yb_2O_3 present in the sample. Thus, the low temperature increase of $\chi(T)$ seems to be intrinsic to these compounds as proven to be so for other MV systems like $CeSn_3$ (Refs. 24 and 25) or $CePd_3$.[24]

The temperature dependence of the electrical resistivity of $Yb_2Ir_3Ga_9$ is shown in Fig. 10(a). Starting from room temperature, $\rho(T)$ drops almost linearly with decreasing temperature. Down to 4.2 K the resistance ratio is $\rho(300\ \text{K})/\rho(4\ \text{K})\simeq 5$. In general, this temperature dependence resembles that of typical Yb-based MV compounds such as $YbCu_4Ga$ (Ref. 26) or $YbInAu_2$,[27] which possess a characteristic temperature $T_K \geqslant 300$ K.

V. ANALYSIS AND DISCUSSION

The present results clearly show that the nature of the GS properties of the Yb-based $R_2T_3X_9$ compounds is given by the X ligand. Whereas the compounds with $X=$Al are found to be trivalent, in those with the isoelectronic $X=$Ga a slight change in the valence of Yb gives rise to a MV-GS. This situation is found for the compounds studied here, formed with $T=$Rh and Ir, as well as for $T=$Co.[28] In the latter case, $Yb_2Co_3Al_9$ orders magnetically at $T_N=1.2$ K, whereas $Yb_2Co_3Ga_9$ shows MV behavior with a maximum in $\chi(T)$ at $T_{\max,\chi}\simeq 50$ K. This behavior can be anticipated from the value of the unit-cell volume, which is clearly lower for $X=$Al (Table I), suggesting a stabilization of the Yb^{3+} configuration with respect to the compounds with $X=$Ga.[29]

Further support to this result can be obtained from an analysis of the coordination polyhedron around the R atoms following the Brunner-Schwarzenbach method,[30] in which all interatomic distances between an atom and its neighbors are plotted in a next-neighbor histogram. From the information of the atomic coordinates of some $R_2T_3X_9$ compounds available in the literature[5,6,8] it is possible to determine that the coordination polyhedron around the R atoms is formed by a total of 11 X ligands as nearest neighbors, and a total of 6 T ligands as next-nearest neighbors. This result seems to be an intrinsic feature of the $Y_2Co_3Ga_9$-type structure and corroborates our observation about the strong influence of the X atoms on the valence state of the $Yb_2T_3X_9$ compounds.

In the following we shall concentrate our discussion on the low-temperature properties of $Yb_2Rh_3Al_9$ and $Yb_2Ir_3Al_9$. Their transport and specific-heat data clearly indicate that the GS properties follow from a competition between Kondo effect, RKKY interaction, and CEF effects. In particular, our $\rho(T)$ and TEP data (cf. Figs. 5, 6, and 7) show a striking similarity to those of $YbCu_4Au$ and $YbCu_4Pd$.[20,31,32] The latter compounds are described as magnetic KL systems with transition temperatures $T_N<1$ K,[33] Kondo temperatures $T_K\simeq 0.5$ K,[34] and low-lying CEF excited levels separated by an energy $\Delta_{\text{CEF}}\simeq 45$ K from the GS doublet.[34] We propose that in the case of $Yb_2Rh_3Al_9$ and $Yb_2Ir_3Al_9$ the respective high-temperature maxima in $\rho(T)$ and minima in TEP are due to the interaction of Kondo-type incoherent scattering on low-lying CEF levels situated at $\Delta_{\text{CEF}}\simeq 30$ K. This is supported by the features observed in the transport properties, where Kondo-type correlations are responsible for the enhanced logarithmic increase of $\rho(T)$ and the enhanced negative values of TEP (cf. Figs. 5, 6, and 7). The same picture also holds for $Yb_2Co_3Al_9$ as well, where the low-temperature transport and thermal properties were observed to be influenced by CEF effects in an analogous way.[28] Thus, the presence of low-lying CEF levels seems to be characteristic of the Yb-based $R_2T_3X_9$ compounds.

Now, in order to get insight into the influence of the Kondo effect on the GS doublet we analyze the C_P/T results in some detail. The enhanced C_P/T values above T_N (i.e., of the order of 300 mJ/mol Yb K^2; cf. Figs. 8 and 9) indicate that the magnetic ordering of these compounds develops from a correlated paramagnetic state. Moreover, the large residual $\gamma_o\simeq 230$ mJ/mol Yb K^2 values are typical of magnetic KL systems in which, due to Kondo compensation, not all the electronic degrees of freedom are condensed into the MO-GS. Further indication of the influence of the Kondo effect is given by the fact that, despite sharp anomalies that occur at T_N, the respective C_P jumps [i.e., $\Delta C_P(T_N)\simeq 6.6$ J/mol Yb K] correspond to only $\simeq$55% of the expected value in a mean-field description [i.e., $\Delta C_P(T_N)=3/2R\equiv 12.5$ J/mol Yb K].[35] This observation is backed

by the value of the entropy gain at $T=T_N$, which is only $\simeq 60\%$ of the expected $R\ln 2$ value for a GS doublet, as shown in Figs. 8(a) and 9(a).

The value of the Kondo temperature T_K for these compounds can be estimated from the C_P data following an approach based on molecular-field calculations for the $S=1/2$ resonant-level model.[36] Within this framework a close relationship between $\Delta C_P(T_N)$ and the ratio between T_K and T_N can be established.[37] This procedure was proved to work out satisfactorily well for a variety of Ce- and Yb-based magnetic KL systems.[37,38] According to this picture, the observed values of $\Delta C_P(T_N)$ correspond to the ratio $T_K/T_N \simeq 0.75$, leading to $T_K \simeq 2.6$ K and $T_K \simeq 4.1$ K for $Yb_2Rh_3Al_9$ and $Yb_2Ir_3Al_9$, respectively. These estimated T_K values are one order of magnitude smaller than the high temperature $\rho(T)$ and TEP anomalies, confirming that the latter are indeed related to CEF effects.

In summary, our results indicate that $Yb_2Rh_3Al_9$ and $Yb_2Ir_3Al_9$ can be classified as two heavy-fermion AF systems with competing Kondo and RKKY interactions of similar magnitude (i.e., $T_K \simeq T_{\mathrm{RKKY}}$), leading to γ_o values of ~ 230 mJ/mol Yb K^2 and a reduced entropy gain at T_N. The transport data show evidence of low-lying CEF levels separated by $\Delta_{\mathrm{CEF}} \simeq 30$ K from the GS doublet. On the other hand, the gallides $Yb_2Rh_3Ga_9$ and $Yb_2Ir_3Ga_9$ appear as MV compounds with characteristic temperatures two orders of magnitude larger than those of the Al-based homologues. These relatively large T_K values overcome the CEF splitting and therefore the total degeneracy of the $J=7/2$ multiplet has to be taken into account in order to describe their GS properties.

In the last part of this discussion, we take profit of the variety of members of the $R_2T_3X_9$ series to compare the magnetic properties of a large number of isostructural *f*-electron systems formed with the same T and X ligands. Starting with the known La-based compounds, i.e., $La_2Rh_3Al_9$,[8] $La_2Rh_3Ga_9$, and $La_2Ir_3Ga_9$,[39] they behave as normal metals showing Pauli-type paramagnetism. No superconductivity was detected down to 2 K.[39] On the other hand, the compounds formed with $R=$ Nd and Tb, i.e., $Nd_2Rh_3Al_9$ and $Tb_2Rh_3Al_9$, behave as normal (trivalent) rare-earth based compounds with AF transitions at $T_N=6$ K and 20 K, respectively,[39] in agreement with their respective De Gennes's factors.

But the most interesting point of comparison to the Yb-based systems is certainly given by the compounds formed with Ce and U, whose properties are expected to depend to a different extent on the hybridization strength $\mathcal{J}$, provided in each case by the environmental conditions around the R atoms. In the case of $R=$ Ce,[7–9] there is a slight systematic increase of the temperature of the high-temperature maxima of the transport properties (i.e., ρ and TEP) from the compounds with $X=$ Ga to those with $X=$ Al (the effect of Al and Ga are inverted in Ce compounds as an indirect consequence of the electron-hole symmetry, Ref. 16). But since these compounds are already in the MV regime, it is not so clear whether $\mathcal{J}$ depends solely on the X ligands or not. However, as stated above, the origin of the heavy-fermion-like behavior observed at lower temperatures remains an open question.

In contrast, the U-based compounds resemble the situation found for $R=$ Yb, namely the GS properties seem to depend mainly on the X ligand. This analogy is observed from their magnetic and transport properties,[7,8] since the compounds with $X=$ Ga show lower transition temperatures and maxima in their transport properties at lower temperatures in comparison with the $X=$ Al counterparts. This observation is emphasized by the fact that $U_2Ir_3Al_9$ and $Yb_2Ir_3Al_9$ possess identical magnetic structures.[14]

As a conclusion, the change of the X ligand strongly influences the hybridization strength and therefore the GS properties of the Yb-based $R_2T_3X_9$. The compounds with $X=$ Al show the typical characteristics of heavy-fermion antiferromagnets, whereas those with isoelectronic $X=$ Ga show MV behavior with an increase in two orders of magnitude in the value of T_K. This is a clear consequence of the sensitivity of Yb to changes in the nearest-neighbor coordination polyhedron formed solely by X ligands. This drastic change in the GS properties for $R=$ Yb contrasts to the smooth trend observed for the Ce-based compounds and might shed light into the formation of heavy fermions in Yb-based systems. In particular, it may give a hint of why Yb-based compounds present either a MO-GS (eventually with a low T_K) or a MV-GS with large T_K values, and therefore it may help to understand why there are extremely few prototypical examples of magnetically nonordered Yb compounds close to a magnetic instability at ambient pressure.

ACKNOWLEDGMENTS

The authors acknowledge G. Ehlers, A. Hiess, S. Coad, J. X. Boucherle, F. Givord, T. Hansen, and E. Suard for kindly providing us unpublished neutron-diffraction results. One of us (O.T.) acknowledges the Alexander-von-Humboldt Foundation for its support.

[1] N.D. Mathur, F.M. Grosche, S.R. Julian, I.R. Walker, D.M. Freye, R.K.W. Haselwimmer, and G.G. Lonzarich, Nature (London) **394**, 39 (1998), and references therein.

[2] Z. Fisk and M.B. Maple, J. Alloys Compd. **183**, 303 (1992).

[3] C. Geibel, U. Klinger, B. Buschinger, M. Weiden, G. Olesch, F. Thomas, and F. Steglich, Physica B **223&224**, 370 (1996).

[4] S. Doniach, Physica B&C **91B**, 231 (1977).

[5] Yu.N. Grin, R.E. Gladyschevskii, O.M. Sichevich, V.E. Zavodnik, Ya.P. Yarmolyuk, and I.V. Rozhdestvenskaya, Kristallografiya **29**, 893 (1984) [Sov. Phys. Crystallogr. **29**, 528 (1984)].

[6] Yu.N. Grin and P. Rogl, Inorg. Mater. **25**, 514 (1989).

[7] B. Buschinger, Ph.D. thesis, Technical University of Darmstadt, 1997.

[8] B. Buschinger, C. Geibel, M. Weiden, C. Dietrich, G. Cordier, G. Olesch, J. Köhler, and F. Steglich, J. Alloys Compd. **260**, 44 (1997).

[9] B. Buschinger, O. Trovarelli, M. Weiden, C. Geibel, and F. Steg-

lich, J. Alloys Compd. **275-277**, 633 (1998).
[10] K.A. Gschneidner, Jr., S.K. Dhar, J.R. Stierman, and T.-W.E. Tsang, J. Magn. Magn. Mater. **47&48**, 51 (1985).
[11] L.C. Gupta, D.E. MacLaughlin, Cheng Tien, C. Godart, M.A. Edwards, and R.D. Parks, Phys. Rev. B **28**, 3673 (1983).
[12] M.J. Besnus, J.P. Kappler, P. Lehman, and A. Meyer, Solid State Commun. **55**, 779 (1985).
[13] A. Amato and J. Sierro, J. Magn. Magn. Mater. **47&48**, 526 (1985).
[14] A. Hiess, S. Coad, B. Buschinger, O. Trovarelli, J.X. Boucherle, F. Givord, T. Hansen, E. Lelievre-Berna, E. Suard, C. Geibel, and F. Steglich, Physica B **259-261**, 340 (1999).
[15] J.D. Thompson and J.L. Lawrence, in *Handbook on the Physics and Chemistry of the Rare Earths*, edited by K.A. Gschneidner, Jr., L. Eyring, G.H. Lander, and G.R. Choppin (North-Holland, Amsterdam, 1994), Vol. 19, p. 383.
[16] C. Schank, U. Tegel, R. Henseleit, A. Grauel, G. Olesch, C. Geibel, G. Cordier, R. Kniep, and F. Steglich, J. Alloys Compd. **207&208**, 333 (1994).
[17] G. Ehlers, A. Hiess, O. Trovarelli, T. Hansen, C. Geibel, and F. Steglich (unpublished).
[18] A. Hiess, S. Coad, B. Buschinger, O. Trovarelli, J.X. Boucherle, F. Givord, T. Hansen, E. Suard, C. Geibel, and F. Steglich (unpublished).
[19] D. Cornut and B. Coqblin, Phys. Rev. B **5**, 4541 (1972).
[20] E. Bauer, E. Gratz, R. Hauser, Le Tuan, A. Galatanu, A. Kottar, H. Michor, W. Perthold, G. Hilscher, T. Kagayama, G. Oomi, N. Ichimiya, and S. Endo, Phys. Rev. B **50**, 9300 (1994).
[21] K.H. Fischer, Z. Phys. B **76**, 315 (1989).
[22] D. Jaccard and J. Sierro, in *Valence Instabilities*, edited by P. Wachter and H. Boppart (North-Holland, Amsterdam, 1982), p. 409.
[23] J.C.P. Klaasse, F.R. de Boer, and P.F. de Châtel, Physica B&C **106**, 178 (1981).
[24] S.H. Liu, in *Handbook on the Physics and Chemistry of the Rare Earths*, edited by K.A. Gschneidner, Jr., L. Eyring, G.H. Lander, and G.R. Choppin (North-Holland, Amsterdam, 1993), Vol. 17, p. 87.
[25] C. Stassis, C.-K. Loong, B.N. Harmon, S.H. Liu, and R.M. Moon, J. Appl. Phys. **50**, 7567 (1979).
[26] E. Bauer, Le Tuan, R. Hauser, E. Gratz, T. Holubar, G. Hilscher, and K. Yoshimura, J. Magn. Magn. Mater. **140-144**, 1247 (1995).
[27] K. Alami-Yadri, H. Wilhelm, and D. Jaccard, Solid State Commun. **108**, 279 (1998).
[28] S.K. Dhar, C. Mitra, P. Manfretti, A. Palenzona, and P. Bonville, Physica B **259-261** 150 (1999).
[29] G. Wortmann, K. Syassen, K.H. Frank, J. Feldhaus, and G. Kaindl, in *Valence Instabilities* (Ref. 22), p. 159.
[30] G.O. Brunner and D. Schwarzenbach, Z. Kristallogr. **133**, 127 (1971); J.L.C. Daams and P. Villars, J. Alloys Compd. **215**, 1 (1994).
[31] R. Casanova, D. Jaccard, C. Marcenat, N. Hamdaoui, and M.J. Besnus, J. Magn. Magn. Mater. **90&91**, 587 (1990).
[32] J. Diehl, H. Davideit, A. Wildbrett, E. Bauer, and S. Horn, Czech. J. Phys. **46**, 2581 (1996).
[33] C. Rossel, K.N. Yang, M.B. Maple, Z. Fisk, E. Zirngiebl, and J.D. Thompson, Phys. Rev. B **35**, 1914 (1987).
[34] P. Bonville, G. Polatsek, J.A. Hodges, P. Imbert, and G. Lebras, Physica B **186-188**, 254 (1993).
[35] See, for example, H.E. Stanley, *Introduction to Phase Transitions and Critical Phenomena* (Clarendon Press, Oxford, 1971), Chap. 6.
[36] K.D. Schotte and U. Schotte, Phys. Lett. **55A**, 38 (1975).
[37] A. Braghta, Ph.D. thesis, University of Strasbourg, 1989.
[38] M.J. Besnus, A. Braghta, N. Hamdaoui, and A. Meyer, J. Magn. Magn. Mater. **104-107**, 1385 (1992).
[39] O. Trovarelli, B. Buschinger, and C. Geibel (unpublished).